Article

The Role of Nitrogen Dioxide in the Production of Sulfate during Chinese Haze-Aerosol Episodes

Lijie Li, Michael R Hoffmann, and Agustin J. Colussi

Environ. Sci. Technol., **Just Accepted Manuscript** • DOI: 10.1021/acs.est.7b05222 • Publication Date (Web): 29 Jan 2018

The Role of Nitrogen Dioxide in the Production of Sulfate during Chinese Haze-Aerosol Episodes

*Lijie Li, Michael R. Hoffmann and Agustín J. Colussi**
Department of Environmental Science & Engineering, California Institute of Technology, Pasadena, CA 91125, United States

Haze events in China megacities involve the rapid oxidation of SO_2 to sulfate aerosol. Given the weak photochemistry taking place in these optically thick hazes, it has been hypothesized that SO_2 is mostly oxidized by NO_2 emissions in the bulk of pH > 5.5 aerosols. Since $NO_2(g)$ dissolution in water is very slow and aerosols are more acidic, we decided to test such hypothesis. Herein, we report that > 95% $NO_2(g)$ disproportionates: $2\ NO_2(g) + H_2O(l) = H^+ + NO_3^-(aq) + HONO$ (R1), upon hitting the surface of $NaHSO_3$ aqueous microjets exposed to $NO_2(g)$ for < 50 μs, thereby giving rise to strong NO_3^- (m/z = 62) signals detected by online electrospray mass spectrometry, rather than oxidizing HSO_3^- (m/z = 81) to HSO_4^- (m/z = 97) in the relevant pH 3-6 range. Since $NO_2(g)$ will be consumed via R1 on the surface of typical aerosols, the oxidation of S(IV) may in fact be driven by the $HONO/NO_2^-$ generated therein. S(IV) heterogeneous oxidation rates are expected to primarily depend on the surface density and liquid water content of the aerosol, which are enhanced by fine aerosol and high humidity. Whether aerosol acidity affects the oxidation of S(IV) by $HONO/NO_2^-$ remains to be elucidated.

es-2017-05222n-R2

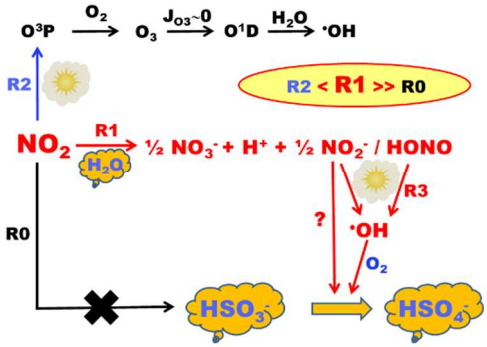
O3P
O2
O3
JO3~O
O1D
H2O
·OH
R2
R2 < R1 >> R0
NO2
R1
½ NO3- + H+ + ½ NO2- / HONO
H2O
R3
?
·OH
O2
R0
HSO3-
HSO4-

TOC

1. Introduction

Chinese megacities often experience haze events (HE)[1-7] that severely impair visibility and induce acute health effects.[5-6, 8-11] Hazes mainly consist of sulfate aerosols produced in the atmospheric processing of SO_2 and NO_2 emissions under particularly adverse meteorological conditions.[12-14] Current models of chemistry in HE significantly underestimate sulfate formation revealing that the mechanism of SO_2 oxidation is not well understood.[15-17] The drastic attenuation of actinic radiation in hazes,[18-21] suggests that SO_2 is oxidized by NO_2(g) in heterogeneous processes on the aerosol itself, rather than in the gas-phase by photogenerated oxidants. The details of such process are uncertain.

Known SO_2 atmospheric oxidation pathways include gas-phase reactions with OH-radicals and stabilized Criegee intermediates, and aqueous phase reactions with O_3,[22] H_2O_2, organic peroxides, NO_x, as well as autoxidation catalyzed by transition metal ions. The low concentrations of photogenerated oxidants[18, 23-30] implies that the chemistries of SO_2 and NO_2 in HE are intertwined. These observations have led to hypothesizing that HSO_3^-(aq) is rapidly oxidized by the NO_2(g) dissolved in aqueous aerosol phases assumed to be at pH > 5.5, reaction R0:

$$2\ NO_2(aq) + HSO_3^-(aq) + H_2O(l) = 2\ H^+(aq) + HSO_4^-(aq) + 2\ NO_2^-(aq) \qquad (R0)$$

on the basis of R0 rates measured in bulk water.[31, 32, 33] Good agreement between field observations and model results on sulfate aerosol formation in HE could be obtained by assuming that R0 proceeds on the surface pH > 5.5 aqueous aerosols at the rates previously reported at pH ~ 6 in bulk water.[31-34] However, the assumptions that aerosols are at pH > 5.5, and NO_2(g) dissolves in large surface-to-volume aerosol droplets as NO_2(aq) as it does in bulk water may not apply.[35-45] Most recent studies suggest that HE aerosols are in fact in the pH 3-5

range.[46-52] Previous laboratory experiments have shown that collisions of ppm $NO_2(g)$ (i.e., in the absence of N_2O_4) with the surface of aqueous electrolyte solutions (*but not on the surface of pure water*) yield $NO_3^-(aq)$ via a first-order in $[NO_2]$ hydrolytic disproportionation catalyzed by anions, reaction R1.[42, 45]

$$2\ NO_2(g) + H_2O(l) = H^+ + NO_3^-(aq) + HONO \qquad (R1)$$

The facts that $NO_2(g)$ is weakly soluble in pure water (Henry's law constant H ~ 0.01 M atm^{-1}) and its uptake coefficient on pure water very small: $\gamma \sim 1 \times 10^{-7}$,[53] its dissolution) in water is unfavorable both by kinetic and thermodynamic reasons. The aqueous phase of most atmospheric aerosols, however, is not pure water. In 2009, we found that anions greatly enhance $NO_2(g)$ uptake on water. The rate determining step involves the capture of $NO_2(g)$ by anions X^- as $X\text{-}NO_2^-$ at air-aqueous interfaces,[42, 45] followed by the reaction of $X\text{-}NO_2^-$ with a second $NO_2(g)$. This phenomenon accounts for the outstanding discrepancy (by a ~ $10^{3\text{-}4}$ factor) between the $NO_2(g)$ uptake coefficients measured in neat water[41, 53] vs those determined on NaCl-seeded droplets in a cloud chamber.[35, 39, 54] Since HE aerosols naturally contain organic and inorganic anions, the expectation was that the fate of $NO_2(g)$ would be determined by R1 at the relevant aerosol air-aqueous interfaces.

Given the societal and economic impact of HE, we deemed important to elucidate the actual role of $NO_2(g)$ in the production of sulfate aerosol under relevant conditions. Herein we report experiments in which aqueous 1 mM $NaHSO_3$ microjets (containing 3 mM of added EDTA to inhibit the potential autoxidation of HSO_3^- catalyzed by pervasive transition metal ions) ejected from a stainless steel syringe are exposed to 5 ppm $NO_2(g)$ for ≤ 50 μs in 1 atm of $N_2(g)$ at 298 K. Reactant and product ions formed on the outermost water layers of the liquid microjets are detected within 1 ms by online electrospray ionization mass spectrometry (o-ESI-MS). This

technique has been used in our laboratory to investigate a suite of gas-liquid reactions at the air-water interface.[55-61] The analysis of our experimental results focuses on the fate of NO_2(g), and the competition between R0 vs R1 during NO_2(g) collisions with the surface of aqueous HSO_3^- solutions under conditions relevant to HE. To our knowledge, this is the first study to provide direct experimental evidence on the extent of S(IV) oxidation by NO_2(g) on the surface of aqueous electrolyte solutions over a wide pH range.

2. Methods

Reactive interactions of NO_2(g) with HSO_3^-(aq) are investigated on the fresh surface of continuously flowing HSO_3^-(aq) microjets that are crossed by NO_2(g)/N_2(g) beams in the spray chamber of an electrospray ionization (ESI) mass spectrometer maintained at 1 atm of N_2(g), and 298 K (Agilent 1100 Series G2445A Ion Trap LC-MS-MSD) (Figure 1). This experimental setup has been described in more detail in previous reports from our laboratory.[44-45, 55, 57-58, 60-64] Aqueous 1 mM $NaSO_3H$ solutions (containing 3 mM EDTA to chelate pervasive traces of transition metal ions known to catalyze HSO_3^- autoxidation) are pumped at 50 μL min^{-1} through an electrically grounded stainless steel needle injector (100 μm bore). These liquid microjets are intersected by beams of NO_2(g) diluted in N_2(g) at controlled flow rates (MKS). Gas-liquid encounters take place during $\tau \leq 50$ μs contact times, which correspond to the estimated lifetimes of the intact microjets prior to their breakup by the nebulizing gas. The outermost layers of the liquid microjets issuing (at 11 cm s^{-1}) from the tip of the syringe are pneumatically stripped and nebulized into charged microdroplets by N_2(g) flowing at > 250 m s^{-1} through a coaxial sheath. Anions contained in the charged microdroplets are detected by online ESI mass spectrometry in the m/z 50-100 range. Anion detection was optimized by setting the drying gas temperature at 325 °C, and the capillary voltage at 3250 V. Fresh solutions were prepared with Milli-Q water

(18.2 MΩ·cm at 25 °C) that had been sparged with N_2(g) for 8 h to remove dissolved O_2 (except as indicated) within 5 minutes prior to injection, in a glove box at < 1 ppm O_2(g). The pH of solutions was adjusted by adding NaOH(aq) or HCl(aq) and measured with a calibrated pH-meter. Throughout, reported pH values correspond to those measured in the bulk of solutions. Sodium bisulfite solution (40% w/w, Sigma-Aldrich), hydrochloric acid (> 30% w/w, Sigma-Aldrich), sodium hydroxide (≥ 99.0 %, Sigma-Aldrich), and ethylenediaminetetraacetic acid (EDTA, > 99.0 %, Sigma-Aldrich), and 48.75 ± 2 % ppm NO_2(g) in N_2(g) (Airgas), were used as received. The actual NO_2(g) concentration at the surface of the aqueous microjets is 10 times smaller (5 ppm) due to dilution by the nebulizer gas.

Figure 1. Schematic diagram of the experimental setup. MFC is the mass flow controller.

3. Results

3. 1 HSO_3^- mass spectral intensities on aqueous surfaces

HSO_3^- m/z = 81 mass spectral signal intensities (I_{81}, normalized to their maximum value, $I_{81,max}$) measured by o-ESI-MS at the gas-aqueous interface of 1 mM $NaHSO_3$ aqueous microjets as functions of bulk pH are shown as blue datapoints in Figure 2. The red trace corresponds to $[HSO_3^-]/[HSO_3^-]_{max}$ values calculated from reported acidity constants in bulk water: pK_{a1} ($H_2O{\cdot}SO_2 \rightleftharpoons HSO_3^- + H^+$) = 1.8, pKa_2 ($HSO_3^- \rightleftharpoons SO_3^{=} + H^+$) = 7.2. Experimental mass spectral data clearly display HSO_3^- deficits at pH < 5 relative to calculated values, which are due to SO_2 losses to the gas-phase. This is considered a feature particular to the HSO_3^-/SO_2 system because the titration curves of less volatile acids and bases determined in this setup were in accordance

with bulk pK_a values.[58, 65] The experimental HSO_3^- signal intensities vs pH data of Fig. 2 provide the reference for analyzing the extent of S(IV) oxidation in the following sections.

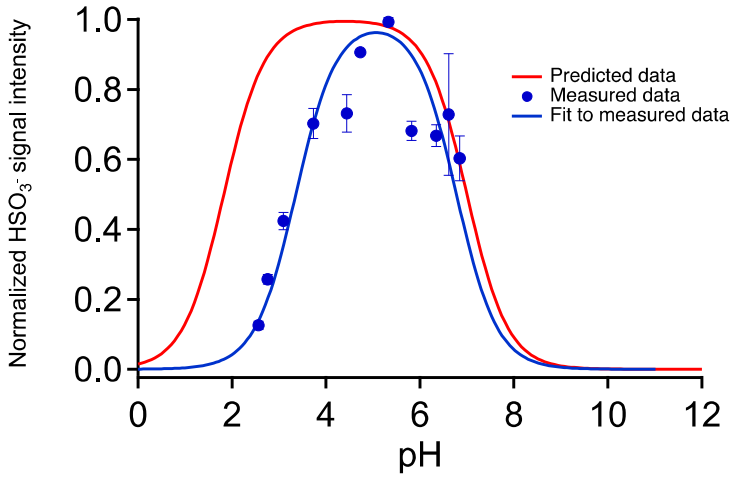

Figure 2. Normalized m/z = 81 (HSO_3^-) signals measured by o-ESI-MS on the surface of aqueous 1 mM $NaHSO_3$(aq) microjets as a function of bulk pH (blue symbols and line). HSO_3^- mole fractions calculated from pK_{a1} ($H_2O{\cdot}SO_2 \rightleftharpoons HSO_3^- + H^+$) = 1.8, pK_{a2} ($HSO_3^- \rightleftharpoons SO_3^= + H^+$) = 7.2 in bulk water (red line).

3. 2 NO_2(g) reactions on aqueous electrolyte surfaces

Mass spectra acquired before and during exposure of pH ~ 5 (1mM HSO_3^- + 3 mM EDTA) aqueous microjets to 5 ppm NO_2(g) for ≤ 50 μs are shown in Figure 3. The main feature is the appearance of a strong NO_3^- m/z = 62 signal, in contrast with the minimal variations displayed by both HSO_3^- m/z = 81 and HSO_4^- m/z = 97 signals upon NO_2(g) exposure. This outcome means that NO_2(g) molecules hitting the surface of pH ~ 5 HSO_3^- microjets mainly undergo fast (within 50 μs) disproportionation, leaving barely any NO_2 for diffusing into the bulk liquid and, supposedly, participate in R0. The following section explores the effect of pH on the competition between R0 and R1.

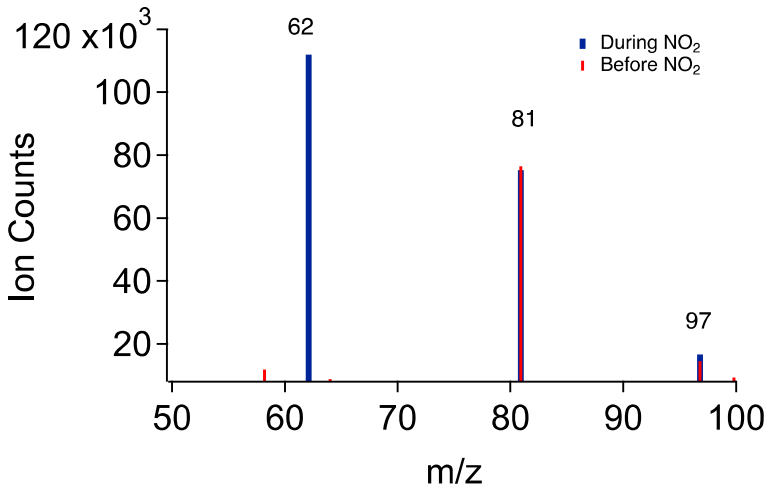

Figure 3. ESI mass spectra of the surface of aqueous 1 mM $NaHSO_3$ + 3 mM EDTA, pH ~ 5 microjets before and after exposure to 5 ppm NO_2(g). Note the presence of minor HSO_4^- (m/z = 97) impurities in the initial solutions.

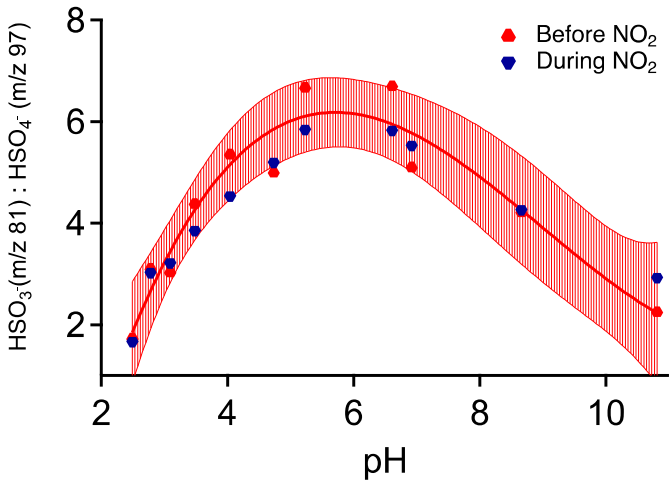

Figure 4. Red symbols, line and 95% confidence band correspond to the ratio of HSO_3^-/HSO_4^- = I_{81}/I_{97} signal intensities on the surface of (1 mM $NaHSO_3$ + 3 mM EDTA in N_2(g)-sparged MQ water) microjets as a function of bulk pH. Blue symbols: after exposure to 5 ppm NO_2(g) for < 50 μs.

3. 3 The oxidation of S(IV) on aqueous surfaces

The extent of HSO_3^-(aq) oxidation by NO_2(g), expressed as the ratio of $[HSO_3^-]/[HSO_4^-] \propto I_{81}/I_{97}$ signal intensities, as a function of pH is shown in Figure 4. I_{81} values correspond to measured I_{81} signals corrected for the depressing effect of the NO_3^- simultaneously produced via R1 at the air-aqueous interface (see below).[63, 66] Figure 4 clearly shows that the extent of HSO_3^- (aq) oxidation via R0 is minimal throughout, barely exceeding experimental error in the pH 3-6 range relevant to HE.

We quantified the fraction of NO_2(g) that oxidizes HSO_3^-(aq) at the air-aqueous interface as f_{R0}, defined by equation E1. In E1, Δ_{81}' is calculated from the decrease of measured I_{81} signals, Δ_{81}, corrected for the NO_3^- depressing effect mentioned above, which is multiplied by the ratio: $\beta = I_{62}/I_{82}$, of the o-ESI mass spectral measured in (1 mM HSO_3^- + 1 mM NO_3^-) equimolar solutions at each pH to convert I_{81} decrements into equivalent Δ_{62} NO_3^- changes.

$$f_{R0} = \frac{\Delta_{81}'}{\Delta_{81}' + \Delta_{62}} \quad \text{(E1)}$$

We found that f_{R0} increases from < 6 % within pH 3.0 and 6.0 up to 42% at pH 10.8. It also increases with acidity up to 16 % at pH 2.5 (Figure 5). This finding means that the anion-catalyzed hydrolytic disproportionation of NO_2(g) on aquated aerosol surfaces, reaction R1, will outcompete R0 throughout, particularly under atmospherically relevant acidic conditions.[35, 39, 41, 43, 45, 57] We have shown that most electrolytes increase the uptake coefficient of NO_2(g) from $\gamma < 1.0 \times 10^{-7}$ in pure water,[37] up to $\gamma = 1 \times 10^{-3}$ - 1×10^{-4} at air-aqueous electrolyte interfaces.[35, 39, 41, 45, 57] The mechanism of enhancement involves trapping NO_2(g) by X^- as $X\text{-}NO_2^-$ at the air-water interface, which can react further with NO_2(g).[45] This interfacial process is expected to dominate the fate of NO_2(g) during HE due to the large surface-to-volume ratio of aerosol microdroplets. We have previously shown that the decay of NO_2(g) on aqueous aerosols via reaction R1

accounts for the similar ~ 4 h NO_2(g) decay half-lives measured by satellite sightings of urban plumes over world megacities ranging from Singapore to Moscow latitudes.[42] We pointed out that if, as generally assumed, NO_2(g) were removed by gas-phase OH-radicals via: NO_2(g) + ·OH(g) = HNO_3(g), much longer decay half-lives should have been observed in winter and at high latitudes, given that "OH-radicals follow the sun".[67]

Next, we performed experiments in which we analyzed, within 5 min via o-ESI-MS, freshly prepared HSO_3^- solutions in air-saturated water without added EDTA.We detected $SO_3^{\bullet -}$ m/z = 80 signals that increase linearly with pH (Figure S3). The formation of $SO_3^{\bullet -}$ is ascribed to the autoxidation of HSO_3^- catalyzed by the omnipresent traces of transition metal ions in our solutions.[68] Whether this process makes a significant contribution to the oxidation of S(IV) under HE conditions is the subject of further studies.[69-70] Additonal experiments carried out by exposing such HSO_3^- solutions (in air-saturated deionized water without added EDTA) to NO_2(g), Figure S4, led to I_{81}/I_{97} ratios similar to those of Figure 4 results NO_2(g), meaning that NO_2 makes negligible contributions to S(IV) autoxidation in our 50 μs timeframes.

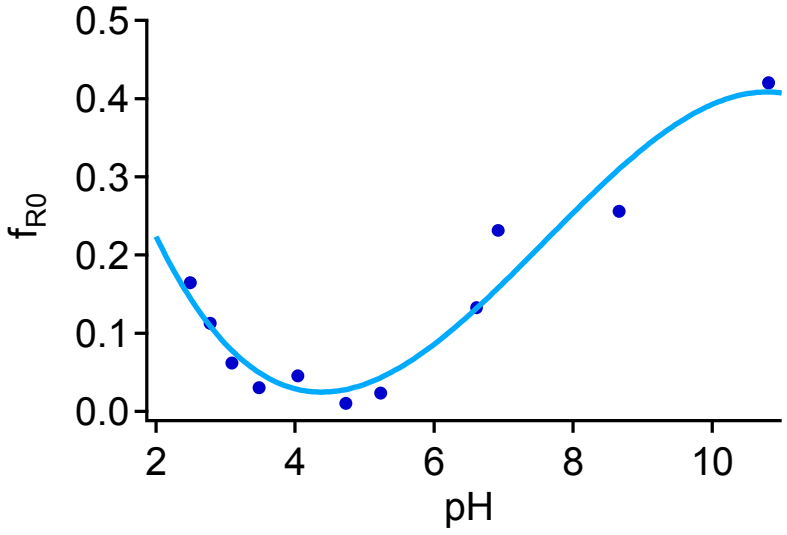

Figure 5. The fraction of NO_2(g) that contributes to S(IV) oxidation, f_{R0} (equation E1) as a function of pH.

4. Discussion

4. 1 Indirect role of NO_2(g) in the oxidation of S(IV)

Our findings open up new perspectives on the mechanism of S(IV) oxidation by NO_2(g) during HE. They underscore the fact that the stoichiometry of R0 could not account for the formation of NO_3^- in HE.[32-33] This is so because if NO_2(g) were the only available oxidant and, moreover, it were consumed in R0, $N(IV)O_2$ could not be oxidized to $N(V)O_3^-$. Any valid mechanism should explain: (1) how are both $S(IV)O_2$ and $N(IV)O_2$ oxidized to $HS(VI)O_4^-$ and $N(V)O_3^-$, and (2) how is HONO produced.

We analyzed the fate of NO_2(g) by considering its reactive uptake on the aerosol via R1 and its photolysis by scattered solar radiation via R2 under representative HE conditions.

$$NO_2(g) + h\nu\ (\lambda \leq 420\ nm) = O(^3P) + NO \qquad (R2)$$

Rate constants for the reactive uptake of NO_2(g), k_{R1}, were estimated with equation E2 from the kinetic theory of gases.

$$k_{R1} = \tfrac{1}{4}\,\gamma\,v_{NO2}\,(S/V) \qquad (E2)$$

where $v_{NO2} = 3.7 \times 10^2$ m s $^{-1}$ is the mean thermal speed of NO_2(g) at 298 K, $\gamma = 10^{-3}$-10^{-4} is the estimated range of the reactive uptake coefficient of NO_2(g) on the surface of aqueous electrolyte solutions,[45] and S/V (in $\mu m^2\ m^{-3}$) is the surface density of aerosols. Aerosols consist of submicron particles with S/V values up to ~2×10^{-3} m^{-1} during hazy days, and values ~ 5 times smaller in clear days.[33] By assuming that $\gamma = 10^{-3}$, S/V = 2×10^{-3} m^{-1} and 4×10^{-4} m^{-1}, we estimate: $k_{R1} \sim 2 \times 10^{-4}$ s^{-1} and $k_{R1} \sim 4 \times 10^{-5}$ s^{-1} on hazy and clear days, respectively.

The low O_3(g) concentrations measured during HE indicate that the photolysis of NO_2(g), which generates the $O(^3P)$ atoms involved in O_3(g) formation: $O_2 + O(^3P) + M = O_3 + M$, is much reduced due to the severe attenuation of actinic sunlight during HE. We estimated time-

and space-averaged photolysis rate constants, k_{R2}, by using the National Center for Atmospheric Research Tropospheric Ultraviolet Visible (TUV) Radiation Model with environmental parameters within the ranges reported for aerosol optical properties and aerosol radiative forcing parameters (see S.3).[24-25] Our estimates: $(k_{R1})_h/(k_{R2})_h \sim 0.5\text{-}1.2$, $(k_{R1})_c/(k_{R2})_c \sim 0.01\text{-}0.1$ (h = hazy, c = clear), are semi-quantitatively consistent with the above premise, and illustrate how the competition between R1 and R2 shifts from hazy to clear days. (See S.3). However, we consider that TUV calculations on the competition between R1 and R2 only provide a lower bound to $(k_{R1})_h/(k_{R2})_h$, because $NO_2(g)$ is not expected to be uniformly distributed but accumulate in the lower layers of dense hazes, where there is minimal actinic radiation and photochemical activity.

Together, our estimates and experimental results support the view that the leading pathway for $NO_2(g)$ during HE is its heterogeneous disproportionation into (NO_3^- + HONO/NO_2^- + H^+) via R1. Note that R1 is autocatalytic because it ultimately contributes to increase the mass and S/V of the aerosols on which it takes place. The rapid development of HE is in fact consistent with such an autocatalytic process. The fact that relative humidity increments are tracked by increased particle number concentrations and surface area density S/V ($\mu m^2\ m^{-3}$) of $PM_{2.5}$, particularly in the accumulation mode, also support the notion that the liquid particles present under such conditions grow from autocatalytic heterogeneous processes.[71]

R1 accounts for the direct formation of NO_3^- and HONO, and would also account for the formation of HSO_4^- if the HONO/NO_2^- produced in R1 could ultimately oxidize S(IV) (see Figure 6).[72-78] As a result, since $f_{R0} \leq 0.1$ in the realistic pH 3 - 6 range, i.e., nearly independent of pH (Figure 5), the acidity/basicity of HE aerosols could be a relevant parameter to S(IV) oxidation rates *if subsequent processes were to depend on aerosol pH*. [79-80] Therefore, our conclusion that the main pathway for $NO_2(g)$ in HE is R1 will stand regardless of future

assessments of aerosol pH. The parameters that may affect a heterogeneous process such as R1 could be a combination of aerosol S/V and aerosol liquid water content, both of which depend on relative humidity.[79-80] We suggest that the apparent dependence of sulfate formation rates on ammonia neutralization of aerosol particles may be the result of cross-correlations between aerosol acidity and the actual causal parameters. In this connection, we wish to point out that the enhancing "ammonium" effect on the oxidation rates of $SO_2(g)$ by $NO_2(g)$ on aqueous solutions might be due to the presence of HSO_4^- anions that capture $NO_2(g)$ at the aerial interface, as explained above.[33] It is also important to realize that Clifton et al., results on the homogeneous reaction rates of $HSO_3^-(aq)$ with the $NO_2(aq)$ produced in situ within bulk solution via $NO_2^-(aq)$ radiolysis,[54] are not applicable to the heterogeneous processes being considered here, which involve $NO_2(g)$ as reactant.

4. 2 HONO/NO_2^- as S(IV) oxidizers

Aqueous HONO and NO_2^- can oxidize HSO_3^- to HSO_4^- in the pH 3-5 range of HE aerosols. HONO and NO_2^- reductions to NO: $E°(HONO + H^+ + e = NO + H_2O) = 0.75$ V, $E°(NO_2^- + 2\ H^+ + e = NO + H_2O) = 1.08$ V or to N_2O: : $E°(2\ HONO + 4\ H^+ + 4e = N_2O + 3\ H_2O) = 1.06$ V, $E°(2\ NO_2^- + 6\ H^+ + 4e = N_2O + 3\ H_2O) = 1.04$ V, could also drive the thermal (dark) oxidation of HSO_3^- to HSO_4^-: $E°(HSO_3^- + H_2O = HSO_4^- + 2\ H^+ + 2e) = 0.15$ V at pH 4, depending on concentrations of reactants and products. The oxidation of HSO_3^- by HONO/NO_2^- however, is complex and proceeds slowly via a free radical mechanism through S- and N-containing intermediates.[81-83] In the presence of air, O_2 could participate in this process (see below).[84]

HONO and NO_2^-, however, could also produce ·OH radicals at significant rates via photolysis, even in optically thick hazes. Estimates made by using the TUV Radiation Model show that the photolysis of HONO (from R1), reaction R3,

$$HONO + h\nu\ (\lambda \leq 390\ nm) = NO + \cdot OH \qquad (R3)$$

is a stronger source of OH-radicals than the photolysis of O_3(g) even at the [HONO] = 0.01[O_3] relative abundances measured during HE.[28] This is due to the much larger solar irradiance in the $\lambda \leq 390$ nm actinic range compared with that in the $\lambda \leq 310$ nm range where O_3(g) dissociates into $O(^1D)$: $O_3 + h\nu = O_2 + O(^1D)$. Our estimates furthermore suggest that OH-radical production rates from HONO during hazy and clear days could comparable, because faster production and slower HONO photolysis under haze conditions are compensated by slower production and faster HONO photolysis in clear days. (Table. S1, S.3). We therefore suggest that ·OH production from HONO photolysis during HE could play a significant role in sulfate formation.[85]

However, since $pK_a(HONO) \sim 3$,[86] some N(III) will be also present as NO_2^-(aq) in the pH = 3-5 range. The photolysis of NO_2^-(aq) also produces ·OH, but at much lower rates that HONO(g), both because of the integrated molar absorptivity of $NO_2^- \sim 15$ times smaller than that of HONO, and the quantum yield of ·OH production: $\phi(NO_2^-(aq) \rightarrow \cdot OH) \sim 0.04$ is 25 times smaller than $\phi(HONO(g) \rightarrow \cdot OH) = 1.0$,[87] due to solvent cage effects. Since the reaction of HSO_3^- with ·OH from the photolysis of HONO/NO_2^-, and presumably as well as the thermal (dark) reaction between NO_2^- + HSO_3^-, both proceed via free radicals, O_2 is expected to participate in these processes and lead to chain oxidation mechanisms.

The preceding considerations leads us to suggest that NO_2(g) oxidizes S(IV) indirectly via the free radical mechanism shown below, rather than directly via R0.

$$2\ NO_2 + H_2O = H^+ + NO_3^- + HONO \qquad (i)$$

$$HONO + h\nu = NO + \cdot OH \qquad (ii)$$

$$\cdot OH + HSO_3^- + O_2 = HSO_4^- + HOO\cdot \qquad (iii)$$

289 $$\cdot OH + RH + O_2 = RO_x + HOO\cdot \quad \text{(iv)}$$

290 $$HOO\cdot + NO = NO_2 + \cdot OH \quad \text{(v)}$$

291 $$NO_2 + HSO_3^- + O_2 + H_2O = NO_3^- + HSO_4^- + H^+ + \cdot OH \quad \text{(R4)}$$

292 Steps (iii) and (iv) as written are not elementary reactions but may proceed via R-OO· and H-
293 OO· intermediates. The overall stoichiometry of R4 indicates that NO_2 and HSO_3^- produce
294 equimolecular amounts of NO_3^- and HSO_4^-, plus an ·OH radical that can oxidize HSO_3^- as well as
295 other species, RH. If ·OH reacts with organics RH instead of HSO_3^-, the HOO· produced in (iv)
296 will regenerate ·OH react via (v) as long as there is sufficient NO remaining. Therefore, although
297 NO_2 may not be the direct oxidizer of SO_2 during HE, the oxidative capacity of the atmosphere
298 will still be determined by initial NO_2 concentrations. As noted above, a related thermal chain
299 oxidation mechanism may be initiated by (NO_2^- + HSO_3^-).

300

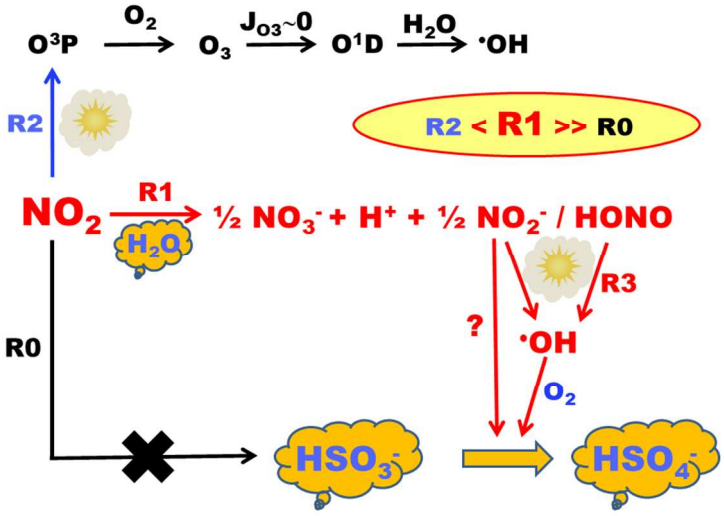

301
302
303 **Figure 6. NO_2 reactions and their impact on S(IV) oxidation during haze aerosol events.**
304

305 **4. 3 Atmospheric Implications**

306 This work focused on the particular heterogeneous chemistry that takes place during the
307 severe wintertime haze events (HE) observed in major Chinese cities. We show that the rapid

formation of sulfate aerosol during HE cannot be due to the direct reaction of HSO_3^- with NO_2. Instead, S(IV) could be oxidized indirectly by NO_2 via the HONO/NO_2^- produced in its fast hydrolytic disproportionation: $2\ NO_2(g) + H_2O(l) = H^+ + NO_3^-(aq) + HONO$ (R1), a process that is catalyzed by anions at air-aqueous aerosol interfaces. The proposed mechanism naturally accounts for the formation of NO_3^- in the aerosol phase, and the significant concentrations of HONO in the gas-phase reported by all field studies. It is expected to be favored at the high relative humidity and high S/V aerosol densities prevalent in HE. We show that the photolysis of HONO and NO_2^- can be a significant source of OH-radicals even under hazy conditions, and point out that the thermal reaction between NO_2^- and HSO_3^- also proceeds via free radicals,[82] both of which can initiate oxidative chains in the presence of O_2. Present findings suggest that future field campaigns should focus on OH-radical measurements during winter HE, an issue that has not been properly addressed in the literature. The main insight is that the relevant parameters for a heterogeneous process such as R1 are the surface density S/V of aerosol hazes, which is related to particle size distributions and the fluidity of the interfacial layers, rather than the acidity of aerosol particles. The apparent dependence of sulfate formation rates on ammonia neutralization of aerosol particles may be the result of cross-correlations between aerosol acidity and the actual causal parameters. Whereas it remains true that the oxidation of SO_2 during HE is driven by primary NO_2 emissions, our work, by clarifying the actual mechanism by which this process is initiated, could guide future research efforts and help optimize future air pollution control strategies.

Summing up: the direct reaction of $NO_2(g)$ with HSO_3^- on the surface of aqueous aerosols is insignificant in the pH 3 to 6 range. On the surface of aqueous electrolyte solutions, such as those of HE aerosols, $NO_2(g)$ is mainly converted to NO_3^- plus HONO/NO_2^- via hydrolytic

disproportionation. The implication is that the oxidation of HSO_3^- during HE coul be mostly due to thermal (dark) and/or photochemical reactions initiated by $HONO/NO_2^-$. The acidity/basicity of HE aerosols could be a relevant parameter to S(IV) oxidation rates only if such processes were to depend on aerosol pH.

Supporting Information: Additional Figures S1 to S4. Explanatory note S0. TUV calculations S1. Estimated rates of HONO and OH production: S2 and Table S1.

Acknowledgments: We acknowledge funding support from National Science Foundation (Grants AC-1238977 & AGS-1744353).

* Corresponding author: ajcoluss@caltech.edu

References

1. Ma, J.; Chen, Y.; Wang, W.; Yan, P.; Liu, H.; Yang, S.; Hu, Z.; Lelieveld, J., Strong Air Pollution Causes Widespread Haze□Clouds over China. *J. Geophys. Res. Atmospheres* **2010**, *115*, 10.1029/2009JD013065.
2. Zheng, G.; Duan, F.; Su, H.; Ma, Y.; Cheng, Y.; Zheng, B.; Zhang, Q.; Huang, T.; Kimoto, T.; Chang, D., Exploring the Severe Winter Haze in Beijing: The Impact of Synoptic Weather, Regional Transport and Heterogeneous Reactions. *Atmos. Chem. Phys.* **2015**, *15*, 2969-2983.
3. Zheng, B.; Zhang, Q.; Zhang, Y.; He, K.; Wang, K.; Zheng, G.; Duan, F.; Ma, Y.; Kimoto, T., Heterogeneous Chemistry: A Mechanism Missing in Current Models to Explain Secondary Inorganic Aerosol Formation During the January 2013 Haze Episode in North China. *Atmos. Chem. Phys.* **2015**, *15*, 2031.
4. Kulmala, M., China's Choking Cocktail. *Nature* **2015**, *526*, 497.
5. Fu, H.; Chen, J., Formation, Features and Controlling Strategies of Severe Haze-Fog Pollutions in China. *Sci. Total Environ.* **2017**, *578*, 121-138.
6. Lin, M.; Tao, J.; Chan, C.-Y.; Cao, J.-J.; Zhang, Z.-S.; Zhu, L.-H.; Zhang, R.-J., Regression Analyses between Recent Air Quality and Visibility Changes in Megacities at Four Haze Regions in China. *Aerosol Air Qual. Res.* **2012**, *12*, 1049-1061.
7. Bouarar, I.; Xuemei, W.; Brasseur, G. P., *Air Pollution in Eastern Asia: An Integrated Perspective*. Springer: Cham, Switzerland, 2017.
8. Xu, P.; Chen, Y.; Ye, X., Haze, Air Pollution, and Health in China. *Lancet* **2013**, *382*, 2067.
9. Huang, R.-J.; Zhang, Y.; Bozzetti, C.; Ho, K.-F.; Cao, J.-J.; Han, Y.; Daellenbach, K. R.; Slowik, J. G.; Platt, S. M.; Canonaco, F., High Secondary Aerosol Contribution to Particulate Pollution During Haze Events in China. *Nature* **2014**, *514*, 218-222.
10. Gao, J.; Woodward, A.; Vardoulakis, S.; Kovats, S.; Wilkinson, P.; Li, L.; Xu, L.; Li, J.; Yang, J.; Cao, L., Haze, Public Health and Mitigation Measures in China: A Review of the Current Evidence for Further Policy Response. *Sci. Total Environ.* **2017**, *578*, 148-157.
11. Gao, M.; Guttikunda, S. K.; Carmichael, G. R.; Wang, Y.; Liu, Z.; Stanier, C. O.; Saide, P. E.; Yu, M., Health Impacts and Economic Losses Assessment of the 2013 Severe Haze Event in Beijing Area. *Sci. Total Environ.* **2015**, *511*, 553-561.
12. Liu, Z.; Xie, Y.; Hu, B.; Wen, T.; Xin, J.; Li, X.; Wang, Y., Size-Resolved Aerosol Water-Soluble Ions During the Summer and Winter Seasons in Beijing: Formation Mechanisms of Secondary Inorganic Aerosols. *Chemosphere* **2017**, *183*, 119-131.
13. Guo, S.; Hu, M.; Zamora, M. L.; Peng, J.; Shang, D.; Zheng, J.; Du, Z.; Wu, Z.; Shao, M.; Zeng, L., Elucidating Severe Urban Haze Formation in China. *Proc. Natl. Acad. Sci. U. S. A.* **2014**, *111*, 17373-17378.
14. Quan, J.; Tie, X.; Zhang, Q.; Liu, Q.; Li, X.; Gao, Y.; Zhao, D., Characteristics of Heavy Aerosol Pollution During the 2012–2013 Winter in Beijing, China. *Atmos. Environ.* **2014**, *88*, 83-89.
15. Wang, Y.; Zhang, Q.; Jiang, J.; Zhou, W.; Wang, B.; He, K.; Duan, F.; Zhang, Q.; Philip, S.; Xie, Y., Enhanced Sulfate Formation During China's Severe Winter Haze Episode in January 2013 Missing from Current Models. *J. Geophys. Res. Atmospheres* **2014**, *119*, 10,425–10,440.
16. Li, G.; Cao, J.; Huang, R., A Possible Pathway for Rapid Growth of Sulfate During Haze Days in China. *Atmos. Chem. Phys* **2017**, *17*, 3301-3316.
17. Yu, H.; Ren, L.; Kanawade, V. P., New Particle Formation and Growth Mechanisms in Highly Polluted Environments. *Curr. Pollut. Rep.* **2017**, 1-9.
18. Hu, B.; Zhao, X.; Liu, H.; Liu, Z.; Song, T.; Wang, Y.; Tang, L.; Xia, X.; Tang, G.; Ji, D., Quantification of the Impact of Aerosol on Broadband Solar Radiation in North China. *Sci. Rep.* **2017**, *7*, 44851.
19. Deng, X.; Zhou, X.; Tie, X.; Wu, D.; Li, F.; Tan, H.; Deng, T., Attenuation of Ultraviolet Radiation Reaching the Surface Due to Atmospheric Aerosols in Guangzhou. *Chinese Science Bulletin* **2012**, *57,* 2759-2766.

20. Xia, D.; Chen, L.; Chen, H.; Luo, X.; Deng, T., Influence of Atmospheric Relative Humidity on Ultraviolet Flux and Aerosol Direct Radiative Forcing: Observation and Simulation. *Asia-Pacific J. Atmos. Sci.* **2016**, *52*, 341-352.
21. Quan, J.; Liu, Q.; Li, X.; Gao, Y.; Jia, X.; Sheng, J.; Liu, Y., Effect of Heterogeneous Aqueous Reactions on the Secondary Formation of Inorganic Aerosols During Haze Events. *Atmos. Environ.* **2015**, *122*, 306-312.
22. He, H.; Wang, Y.; Ma, Q.; Ma, J.; Chu, B.; Ji, D.; Tang, G.; Liu, C.; Zhang, H.; Hao, J., Mineral Dust and Nox Promote the Conversion of So2 to Sulfate in Heavy Pollution Days. *Sci. Rep.* **2014**, *4*, 4172.
23. Kulmala, M.; Petäjä, T.; Kerminen, V.-M.; Kujansuu, J.; Ruuskanen, T.; Ding, A.; Nie, W.; Hu, M.; Wang, Z.; Wu, Z., On Secondary New Particle Formation in China. *Frontiers of Environmental Science & Engineering* **2016**, *10*, 8.
24. Che, H.; Xia, X.; Zhu, J.; Li, Z.; Dubovik, O.; Holben, B.; Goloub, P.; Chen, H.; Estelles, V.; Cuevas-Agulló, E., Column Aerosol Optical Properties and Aerosol Radiative Forcing During a Serious Haze-Fog Month over North China Plain in 2013 Based on Ground-Based Sunphotometer Measurements. *Atmos. Chem. Phys.* **2014**, *14*, 2125-2138.
25. Che, H. Z.; Xia, X. G.; Zhu, J.; Wang, H.; Wang, Y. Q.; Sun, J. Y.; Zhang, X. Y.; Shi, G. Y., Aerosol Optical Properties under the Condition of Heavy Haze over an Urban Site of Beijing, China. *Environ. Sci. Pollut. Res.* **2015**, *22*, 1043-1053.
26. Chen, W.; Tang, H. Z.; Zhao, H. M.; Yan, L., Analysis of Aerosol Properties in Beijing Based on Ground-Based Sun Photometer and Air Quality Monitoring Observations from 2005 to 2014. *Remote Sensing* **2016**, *8*, 110; doi:10.3390/rs8020110.
27. Chen, W.; Yan, L.; Ding, N.; Xie, M. D.; Lu, M.; Zhang, F.; Duan, Y. X.; Zong, S., Analysis of Aerosol Radiative Forcing over Beijing under Different Air Quality Conditions Using Ground-Based Sun-Photometers between 2013 and 2015. *Remote Sensing* **2016**, *8*, 510; doi:10.3390/rs8060510.
28. Hou, S. Q.; Tong, S. R.; Ge, M. F.; An, J. L., Comparison of Atmospheric Nitrous Acid During Severe Haze and Clean Periods in Beijing, China. *Atmos. Environ.* **2016**, *124*, 199-206.
29. Sun, L.; Li, R. B.; Tian, X. P.; Wei, J., Analysis of the Temporal and Spatial Variation of Aerosols in the Beijing-Tianjin-Hebei Region with a 1 Km Aod Product. *Aerosol Air Qual. Res.* **2017**, *17*, 923-935.
30. Zhang, Y.; Huang, W.; Cai, T. Q.; Fang, D. Q.; Wang, Y. Q.; Song, J.; Hu, M.; Zhang, Y. X., Concentrations and Chemical Compositions of Fine Particles (PM2.5) During Haze and Non-Haze Days in Beijing. *Atmos. Res.* **2016**, *174*, 62-69.
31. Lee, Y. N.; Schwartz, S. E., Kinetics of Oxidation of Aqueous Sulfur (IV) by Nitrogen Dioxide. In *Precipitation Scavenging, Dry Deposition and Resuspension*, Pruppacher, H. R.; Semonin, R. G.; Slinn, W. G. N., Eds. Elsevier: New York, 1983; Vol. 1, pp 453-466.
32. Cheng, Y.; Zheng, G.; Wei, C.; Mu, Q.; Zheng, B.; Wang, Z.; Gao, M.; Zhang, Q.; He, K.; Carmichael, G., Reactive Nitrogen Chemistry in Aerosol Water as a Source of Sulfate During Haze Events in China. *Science Advances* **2016**, *2*, e1601530; DOI: 10.1126/sciadv.1601530
33. Wang, G.; Zhang, R.; Gomez, M. E.; Yang, L.; Zamora, M. L.; Hu, M.; Lin, Y.; Peng, J.; Guo, S.; Meng, J., Persistent Sulfate Formation from London Fog to Chinese Haze. *Proc. Natl. Acad. Sci. U. S. A.* **2016**, *113*, 13630-13635.
34. Lammel, G.; Cape, J. N., Nitrous Acid and Nitrite in the Atmosphere. *Chem. Soc. Rev.* **1996**, *25*, 361-369.
35. Bambauer, A.; Brantner, B.; Paige, M.; Novakov, T., Laboratory Study of NO2 Reaction with Dispersed and Bulk Liquid Water. *Atmos. Environ.* **1994**, *28*, 3225-3232.
36. Cheung, J. L.; Li, Y. Q.; Boniface, J.; Shi, Q.; Davidovits, P.; Worsnop, D. R.; Jayne, J. T.; Kolb, C. E., Heterogeneous Interactions of NO2 with Aqueous Surfaces. *J. Phys. Chem. A* **2000**, *104*, 2655-2662.
37. Lee, Y. N.; Schwartz, S. E., Reaction-Kinetics of Nitrogen-Dioxide with Liquid Water at Low Partial-Pressure. *J. Phys. Chem.* **1981**, *85*, 840-848.
38. Mertes, S.; Wahner, A., Uptake of Nitrogen-Dioxide and Nitrous-Acid on Aqueous Surfaces. *J. Phys. Chem.* **1995**, *99*, 14000-14006.

441 39. Novakov, T., Laboratory Study of NO_2 Reaction with Dispersed and Bulk Liquid Water - Reply.
442 *Atmos. Environ.* **1995**, *29*, 2559-2560.
443 40. Ponche, J. L.; George, C.; Mirabel, P., Mass-Transfer at the Air-Water-Interface - Mass
444 Accommodation Coefficients of SO_2, HNO_3, NO_2 and NH_3. *J. Atmos. Chem.* **1993**, *16*, 1-21.
445 41. Schwartz, S. E.; Lee, Y. N., Laboratory Study of NO_2 Reaction with Dispersed and Bulk Liquid
446 Water. *Atmos. Environ.* **1995**, *29*, 2557-2559.
447 42. Colussi, A. J.; Enami, S.; Yabushita, A.; Hoffmann, M. R.; Liu, W. G.; Mishra, H.; Goddard, W. A.,
448 Tropospheric Aerosol as a Reactive Intermediate. *Faraday Discussions* **2013**, *165*, 407-420.
449 43. Enami, S.; Hoffmann, M. R.; Colussi, A., Absorption of Inhaled NO2. *J. Phys. Chem. B* **2009**, *113*,
450 7977-7981.
451 44. Kinugawa, T.; Enami, S.; Yabushita, A.; Kawasaki, M.; Hoffmann, M. R.; Colussi, A. J., Conversion
452 of Gaseous Nitrogen Dioxide to Nitrate and Nitrite on Aqueous Surfactants. *Phys. Chem. Chem. Phys.*
453 **2011**, *13*, 5144-5149.
454 45. Yabushita, A.; Enami, S.; Sakamoto, Y.; Kawasaki, M.; Hoffmann, M. R.; Colussi, A. J., Anion-
455 Catalyzed Dissolution of NO_2 on Aqueous Microdroplets. *J. Phys. Chem. A* **2009**, *113*, 4844-4848.
456 46. Liu, M.; Song, Y.; Zhou, T.; Xu, Z.; Yan, C.; Zheng, M.; Wu, Z.; Hu, M.; Wu, Y.; Zhu, T., Fine
457 Particle Ph During Severe Haze Episodes in Northern China. *Geophys. Res. Lett.* **2017**, *44*, 5213–5221.
458 47. Shi, G.; Xu, J.; Peng, X.; Xiao, Z.; Chen, K.; Tian, Y.; Guan, X.; Feng, Y.; Yu, H.; Nenes, A., pH of
459 Aerosols in a Polluted Atmosphere: Source Contributions to Highly Acidic Aerosol. *Environ. Sci.*
460 *Technol.* **2017**, *51*, 4289-4296.
461 48. Weber, R. J.; Guo, H.; Russell, A. G.; Nenes, A., High Aerosol Acidity Despite Declining
462 Atmospheric Sulfate Concentrations over the Past 15 Years. *Nat. Geosci.* **2016**, *9*, 282-285.
463 49. Guo, H.; Nenes, A.; Weber, R. J., The Underappreciated Role of Nonvolatile Cations on Aerosol
464 Ammonium-Sulfate Molar Ratios. *Atmos. Chem. Phys. Discuss.* **2017**, doi.org/10.5194/acp-2017-737.
465 50. Guo, H.; Weber, R. J.; Nenes, A., High Levels of Ammonia Do Not Raise Fine Particle pH
466 Sufficiently to Yield Nitrogen Oxide-Dominated Sulfate Production. *Sci. Rep.* **2017**, *7*, 12109.
467 51. He, K.; Zhao, Q.; Ma, Y.; Duan, F.; Yang, F.; Shi, Z.; Chen, G., Spatial and Seasonal Variability of
468 Pm2. 5 Acidity at Two Chinese Megacities: Insights into the Formation of Secondary Inorganic Aerosols.
469 *Atmos. Chem. Phys.* **2012**, *12*, 1377.
470 52. Xiyuan, C.; Pengzhen, H.; Zhuang Jiang, X. Y.; Fange, Y.; Longquan, W., Aerosol Acidity During
471 Winter Heavy Haze Episodes in Beijing and Gucheng, China. *J. Meteorol. Res.* **2018**, *32*, doi:
472 10.1007/s13351-018-7063-4. (in press)
473 53. Lee, Y. N.; Schwartz, S. E., Reaction-Kinetics of Nitrogen-Dioxide with Liquid Water at Low
474 Partial-Pressure. *J. Phys. Chem.* **1981**, *85*, 840-848.
475 54. Clifton, C. L.; Altstein, N.; Huie, R. E., Rate Constant for the Reaction of Nitrogen Dioxide with
476 Sulfur (IV) over the pH Range 5.3-13. *Environ. Sci. Technol.* **1988**, *22*, 586-589.
477 55. Enami, S.; Colussi, A. J., Criegee Chemistry on Aqueous Organic Surfaces. *J Phys. Chem. Lett.* **2017**,
478 *8*, 1615-1623.
479 56. Enami, S.; Hoffmann, M. R.; Colussi, A. J., Acidity Enhances the Formation of a Persistent Ozonide
480 at Aqueous Ascorbate/Ozone Gas Interfaces. *PNAS* **2008**, *105*, 7365-7369.
481 57. Enami, S.; Hoffmann, M. R.; Colussi, A. J., Absorption of Inhaled NO_2. *J. Phys. Chem. B* **2009**, *113*,
482 7977-7981.
483 58. Enami, S.; Hoffmann, M. R.; Colussi, A. J., Proton Availability at the Air/Water Interface. *J. Phys.*
484 *Chem. Lett.* **2010**, *1*, 1599-1604.
485 59. Enami, S.; Hoffmann, M. R.; Colussi, A. J., OH-Radical Specific Addition to Glutathione S-Atom at
486 the Air-Water Interface: Relevance to the Redox Balance of the Lung Epithelial Lining Fluid. *J. Phys.*
487 *Chem. Lett.* **2015**, *6*, 3935-3943.
488 60. Enami, S.; Sakamoto, Y.; Colussi, A. J., Fenton Chemistry at Aqueous Interfaces. *Proc. Natl. Acad.*
489 *Sci. U. S. A.* **2014**, *111*, 623-628.

490 61. Enami, S.; Vecitis, C. D.; Cheng, J.; Hoffmann, M. R.; Colussi, A. J., Electrospray Mass
491 Spectrometric Detection of Products and Short-Lived Intermediates in Aqueous Aerosol Microdroplets
492 Exposed to a Reactive Gas. *J. Phys. Chem. A* **2007**, *111*, 13032-13037.
493 62. Enami, S.; Hoffmann, M. R.; Colussi, A. J., Molecular Control of Reactive Gas Uptake "on Water".
494 *J. Phys. Chem. A* **2010**, *114*, 5817-5822.
495 63. Enami, S.; Mishra, H.; Hoffmann, M. R.; Colussi, A. J., Hofmeister Effects in Micromolar
496 Electrolyte Solutions. *J. Chem. Phys.* **2012**, *136*, 154707.
497 64. Enami, S.; Vecitis, C. D.; Cheng, J.; Hoffmann, M. R.; Colussi, A. J., Mass Spectrometry of
498 Interfacial Layers During Fast Aqueous Aerosol/Ozone Gas Reactions of Atmospheric Interest. *Chem.*
499 *Phys. Lett.* **2008**, *455*, 316-320.
500 65. Enami, S.; Stewart, L. A.; Hoffmann, M. R.; Colussi, A. J., Superacid Chemistry on Mildly Acidic
501 Water. *J. Phys. Chem. Lett.* **2010**, *1*, 3488-3493.
502 66. Enami, S.; Colussi, A. J., Long-Range Specific Ion-Ion Interactions in Hydrogen-Bonded Liquid
503 Films. *J. Chem. Phys.* **2013**, *138*, 184706.
504 67. Wennberg, P. O., Atmospheric Chemistry: Radicals Follow the Sun. *Nature* **2006**, *442*, 145-146.
505 68. Hung, H. M.; Hoffmann, M. R., Oxidation of Gas-Phase SO2 on the Surfaces of Acidic
506 Microdroplets: Implications for Sulfate and Sulfate Radical Anion Formation in the Atmospheric Liquid
507 Phase. *Environ. Sci. Technol.* **2015**, *49*, 13768-13776.
508 69. Fang, T.; Guo, H. Y.; Zeng, L. H.; Verma, V.; Nenes, A.; Weber, R. J., Highly Acidic Ambient
509 Particles, Soluble Metals, and Oxidative Potential: A Link between Sulfate and Aerosol Toxicity. *Environ.*
510 *Sci. Technol.* **2017**, *51*, 2611-2620.
511 70. Martin, L.; Hill, M.; Tai, A.; Good, T., The Iron Catalyzed Oxidation of Sulfur (IV) in Aqueous
512 Solution: Differing Effects of Organics at High and Low pH *J. Geophys. Res. Atmospheres* **1991**, *96*,
513 3085-3097.
514 71. Liu, Y.; Wu, Z.; Wang, Y.; Xiao, Y.; Gu, F.; Zheng, J.; Tan, T.; Shang, D.; Wu, Y.; Zeng, L.,
515 Submicrometer Particles Are in the Liquid State During Heavy Haze Episodes in the Urban Atmosphere
516 of Beijing, China. *Environ. Sci. Technol. Lett.* **2017**, *4*, 427–432.
517 72. Huang, R. J., et al., Concentration and Sources of Atmospheric Nitrous Acid (HONO) at an Urban
518 Site in Western China. *Sci. Total Environ.* **2017**, *593*, 165-172.
519 73. Li, X., et al., Exploring the Atmospheric Chemistry of Nitrous Acid (HONO) at a Rural Site in
520 Southern China. *Atmos. Chem. Phys.* **2012**, *12*, 1497-1513.
521 74. Li, Y.; An, J.; Kajino, M.; Li, J.; Qu, Y., Impacts of Additional HONO Sources on Concentrations
522 and Deposition of Noy in the Beijing-Tianjin-Hebei Region of China. *SOLA* **2015**, *11*, 36-42.
523 75. Liu, Z.; Wang, Y. H.; Costabile, F.; Amoroso, A.; Zhao, C.; Huey, L. G.; Stickel, R.; Liao, J.; Zhu,
524 T., Evidence of Aerosols as a Media for Rapid Daytime HONO Production over China. *Environ. Sci.*
525 *Technol.* **2014**, *48*, 14386-14391.
526 76. Sörgel, M.; Regelin, E.; Bozem, H.; Diesch, J.-M.; Drewnick, F.; Fischer, H.; Harder, H.; Held, A.;
527 Hosaynali-Beygi, Z.; Martinez, M., Quantification of the Unknown HONO Daytime Source and Its
528 Relation to No 2. *Atmos. Chem. Phys. Discuss.* **2011**, *11*, 15119-15155.
529 77. Tang, Y.; An, J.; Wang, F.; Li, Y.; Qu, Y.; Chen, Y.; Lin, J., Impacts of an Unknown Daytime Hono
530 Source on the Mixing Ratio and Budget of HONO, and Hydroxyl, Hydroperoxyl, and Organic Peroxy
531 Radicals, in the Coastal Regions of China. *Atmos. Chem. Phys.* **2015**, *15*, 9381-9398.
532 78. Wang, L. W., et al., Hono and Its Potential Source Particulate Nitrite at an Urban Site in North China
533 During the Cold Season. *Sci. Total Environ.* **2015**, *538*, 93-101.
534 79. Bian, Y.; Zhao, C.; Ma, N.; Chen, J.; Xu, W., A Study of Aerosol Liquid Water Content Based on
535 Hygroscopicity Measurements at High Relative Humidity in the North China Plain. *Atmos. Chem. Phys.*
536 **2014**, *14*, 6417-6426.
537 80. Tan, H.; Cai, M.; Fan, Q.; Liu, L.; Li, F.; Chan, P.; Deng, X.; Wu, D., An Analysis of Aerosol Liquid
538 Water Content and Related Impact Factors in Pearl River Delta. *Sci. Total Environ.* **2017**, *579*, 1822-1830.
539 81. Martin, L. R.; Damschen, D. E.; Judeikis, H. S., The Reactions of Nitrogen Oxides with SO_2 in
540 Aqueous Aerosols. *Atmos. Environ. (1967)* **1981**, *15*, 191-195.

82. Mendiara, S.; Ghibaudi, E.; Perissinotti, L.; Colussi, A., Free Radicals and Diradicals in the Reaction between Nitrous Acid and Bisulfite in Acid Aqueous Media. *J. Phys. Chem.* **1992**, *96*, 8089-8091.
83. Littlejohn, D.; Wang, Y.; Chang, S. G., Oxidation of Aqueous Sulfite Ion by Nitrogen Dioxide. *Environ. Sci. Technol.* **1993**, *27*, 2162-2167.
84. Oblath, S.; Markowitz, S.; Novakov, T.; Chang, S., Kinetics of the Initial Reaction of Nitrite Ion in Bisulfite Solutions. *J. Phys. Chem.* **1982**, *86*, 4853-4857.
85. Li, Y.; An, J.; Gultepe, I., Effects of Additional HONO Sources on Visibility over the North China Plain. *Advances in Atmospheric Sciences* **2014**, *31*, 1221.
86. Riordan, E.; Minogue, N.; Healy, D.; O'Driscol, P.; Sodeau, J. R., Spectroscopic and Optimization Modeling Study of Nitrous Acid in Aqueous Solution. *J. Phys. Chem. A* **2005**, *109*, 779-786.
87. Chu, L.; Anastasio, C., Temperature and Wavelength Dependence of Nitrite Photolysis in Frozen and Aqueous Solutions. *Environ. Sci. Technol.* **2007**, *41*, 3626-3632.

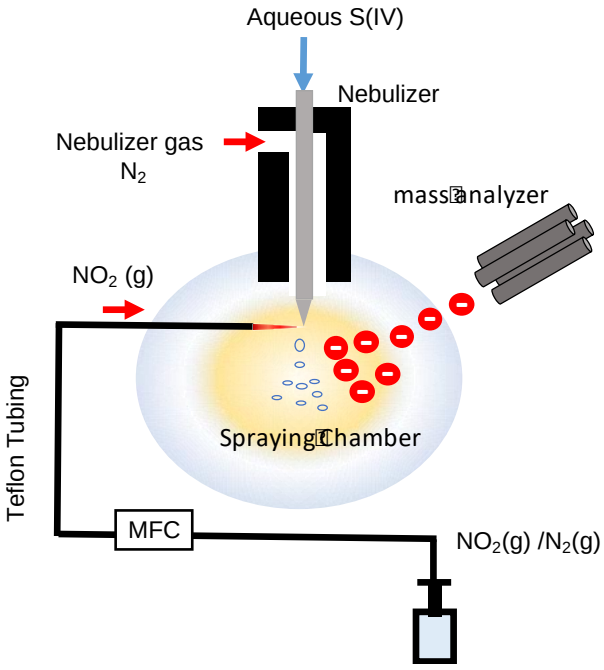

Figure 1. Schematic diagram of the experimental setup. MFC is the mass flow controller.